PAPER • OPEN ACCESS

Simultaneous measurement of surface shape and pressure using structured illumination

To cite this article: Mark K Quinn and Tom B Fisher 2021 *Meas. Sci. Technol.* **32** 024011

View the article online for updates and enhancements.

Simultaneous measurement of surface shape and pressure using structured illumination

Mark K Quinn and Tom B Fisher

Department of Mechanical, Aerospace and Civil Engineering, University of Manchester, Manchester, M13 9PL, United Kingdom

E-mail: mark.quinn@manchester.ac.uk

CrossMark

Abstract

This article describes the successful implementation of a structured UV light field, generated from a modified LCD projector, to excite pressure-sensitive paint (PSP) and measure surface shape simultaneously without the need to compromise the PSP by mechanical degradation of the coating. Using commercially available hardware, results were gathered in a Mach 5 wind tunnel, showing the expected pressure distribution around a cone model with a flare and the surface geometry without any prior knowledge or information. The demonstrated methodology can be used to measure aerodynamic models exhibiting elastic deformation under load during a wind tunnel measurement campaign, providing out-of-plane motions are small. The captured deformation and pressure results can be used to support validation of structural models and correct numerical simulation meshes to the actual shape investigated in the wind tunnel.

(Some figures may appear in colour only in the online journal)

1. Introduction

The use of pressure-sensitive paint (PSP) as an aerodynamic investigation technique has been steadily growing since its formative years in the 1980s and has been developed to give full-surface coverage around transonic vehicles [1–6]. The PSP technique is based on the quenching of luminescence by oxygen, which can be measured as a surrogate for surface pressure through Dalton's law of partial pressure and the well-known Stern–Volmer equation, presented here using higher-order terms to help model non-linearity:

$$\frac{I_{\text{ref}}}{I} = A\left(T\right) + B\left(T\right)\frac{P}{P_{\text{ref}}} + C\left(T\right)\left(\frac{P}{P_{\text{ref}}}\right)^2 \qquad (1)$$

where I is image intensity (counts), P is pressure, the subscript ref denotes a reference condition, and $A\left(T\right)$, $B\left(T\right)$, and $C\left(T\right)$ are calibration coefficients which are functions of temperature. A gas-permeable, or porous, coating is applied to the aerodynamic surface of investigation [7–11] which contains a photoactive molecule known as a luminophore. The luminophore is illuminated at a wavelength which excites it to a higher electronic state. The excited luminophore then returns to its ground state by various paths including emitting light of a longer wavelength. The probability of a light-emitting deactivation path depends on the local levels of oxygen present (higher oxygen concentration results in lower light emission). This is the basic working principle of PSP and has been covered in much more detail by others [7].

Recent developments have extended the range of applicability of the PSP technique to include unsteady cavity flows [12–15], full-surface unsteady measurements [6, 14], transient measurements [16, 17], and highly versatile miniaturised measurements [18, 19]. A thorough description of developments over the past two decades is given in the reviews of
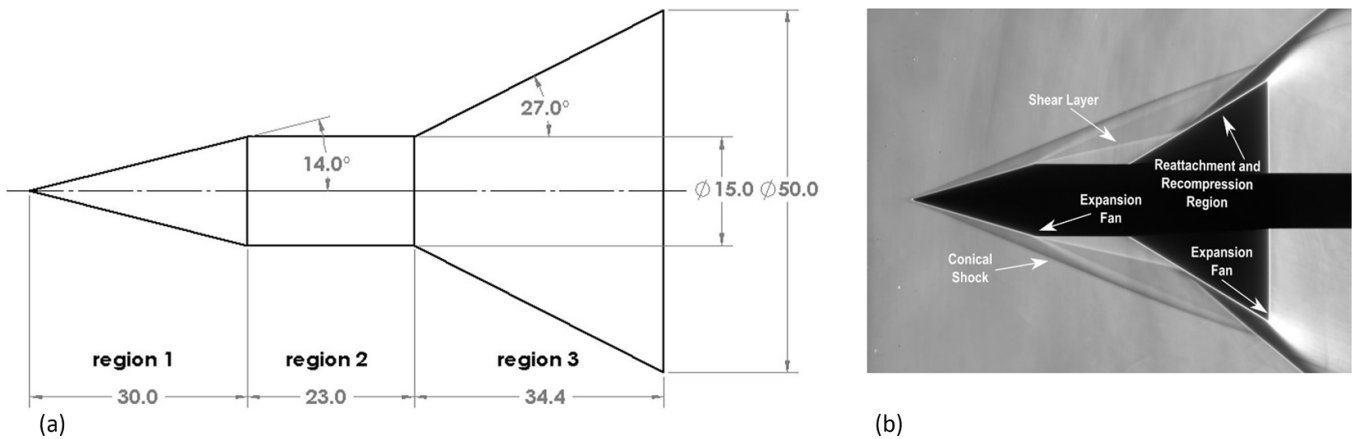
Figure 1. (a) Schematic of the flared cone model (all dimensions in mm); (b) Schlieren image of Mach 5 flow field with features labelled.

Gregory *et al* in 2008 [9] and more recently by Peng and Liu in 2019 [11]. However, a remaining challenge to be solved is model motion, misalignment, and vibration between capturing reference and test condition images (also known as wind-off/-on images). This motion causes inaccuracies in pressure results as the images are no longer aligned with their original position and, as the division shown in equation (1) is a pixel-wise operation, significant errors can arise. Efforts have been made to map images on to meshes prior to the application of equation (1); however, this not only increases the required image processing, but it also does not take into account any model deformation—something which is often an issue, particularly in large facilities [20, 21]. Efforts to counteract the impact of motion and misalignment have been made through the simultaneous (or very rapid sequential) acquisition of a pressure and a reference signal. These approaches, known as self-referencing, can be split into two broad categories: binary or single-shot. The binary approach includes a pressure insensitive component with a different Stokes shift than the pressure-sensitive component of the PSP so it can be measured simultaneously using a colour camera as demonstrated by Sakaue *et al* [22] (even with unsteady illumination [23]). The single-shot approach requires more stringent illumination and image acquisition equipment requirements to reference through lifetime measurements, but has been implemented to great effect by multiple researchers [24–27].

The digital image correlation (DIC)-based image deformation method implemented by Ogg *et al* [28] significantly improved the PSP result uniformity over non-deformed images; highlighting a more robust method of image transformation compared to the more regularly used affine or projective image transformations.

Previous attempts to measure the shape of a model surface and the surface pressure have been successful [29]; however, the method of acquisition of the shape information used custom plenoptic vision cameras, which are expensive and complex to manufacture. Moreover, a texture was required to be applied to the PSP, which meant the coating could not be used again without respraying. Recent studies by Ogg *et al* [28] and Lynch *et al* [30] demonstrated the use of DIC to successfully

capture PSP and surface shape deformation simultaneously for compliant bumps in transonic flow and shock tube testing respectively; however, these studies relied on applying a physical speckle pattern to the model (as a result of using uniform illumination), thereby compromising the PSP. Ravichandran *et al* [31] and Gramola *et al* [32] measured similar compliant structures using binary PSP using photogrammetry targets applied after the PSP layer generating a sparse surface mesh. Applying targets in this way has the potential to be aerodynamically intrusive, particularly in sensitive flows such as transonic shockwave boundary layer interactions. This approach, although successful, did lead to significant image processing artefacts, making interpretation of PSP results more challenging. An alternative approach was recently demonstrated by Dong *et al* [27] who utilised a gridded PSP system, texturing the PSP sprayed on to the surface by using a repeating circular mask followed by a Hough transform-based algorithm to detect and track the circular PSP pattern.

This study utilises a similar approach to that of Ogg *et al* [28] and Lynch *et al* [30]; however, instead of uniform illumination, an incident light texture was applied to the PSP surface using a modified LCD projector which was able to both project a stochastic pattern and provide UV PSP excitation. The response was imaged using two cameras with appropriate filters, enabling a stereoscopic reconstruction of the surface shape as well as the PSP response without compromising the PSP coating. Results are presented for a model tested at Mach 5 in the University of Manchester high supersonic tunnel (HSST) showing accurate and fully calibrated PSP and surface shape information.

2. Methodology

A flared cone model, shown in figure 1(a), was tested in the University of Manchester HSST facility. This model is used as, when tested at Mach 5, it produces strong and weak flow features, as shown in figure 1(b), including very large pressure signals. The model is rigid and does not bend under load; however, measurement of its shape, simultaneously with the surface pressure, demonstrates the feasibility of this technique.
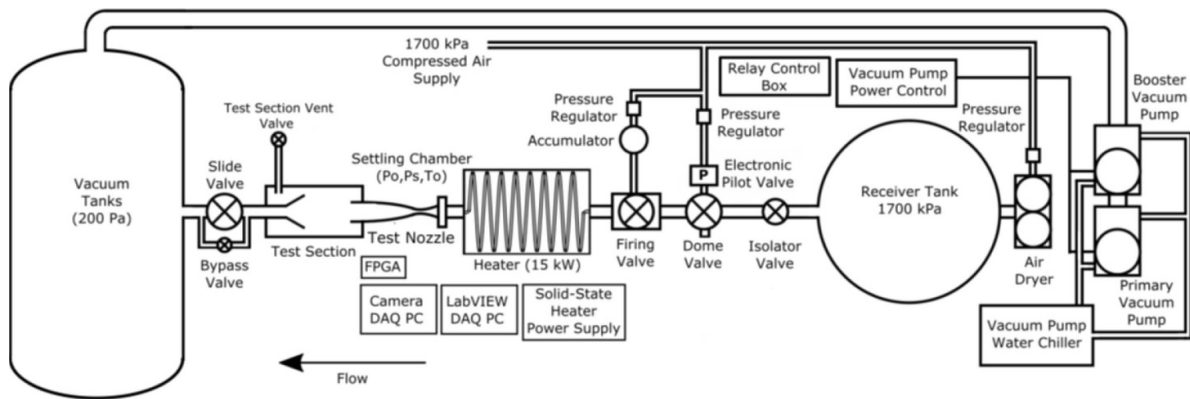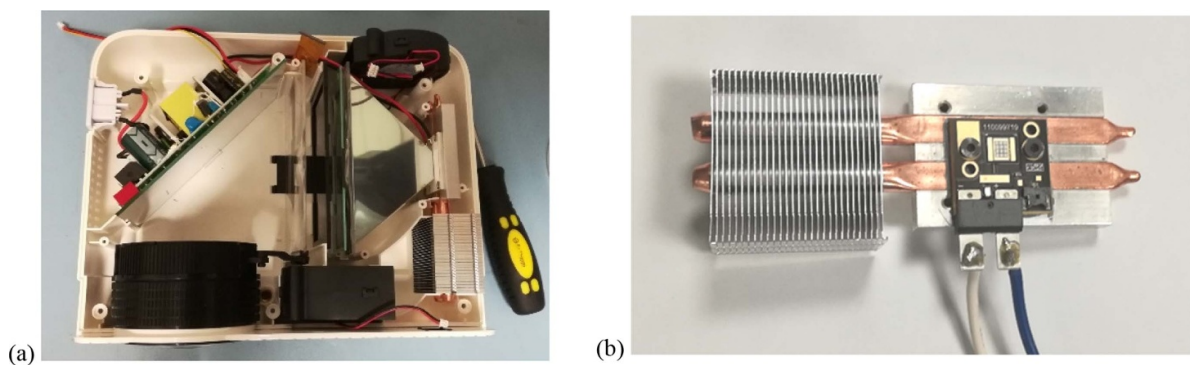
Figure 2. Layout of the HSST.

Figure 3. (a) Partially disassembled projector; (b) Luminus Devices CBM-120-UV-C31-K395 LED installed on the projector cooling assembly.

The flow around this model has been extensively studied by others [29, 33, 34] and will not be described in detail here.

The facility layout, shown in figure 2, consists of a free jet expanding into an evacuated, quiescent plenum chamber. The facility is capable of running at Mach 4, 5, and 6; however, the current experiments were performed at Mach 5. With a maximum total pressure of 8.1 bar and large storage tanks, the facility is capable of providing stable run-times of 7.5 s. The flow is temperature-controlled using a resistive heater connected to a high-current power supply and is capable of generating total temperatures from 288 to 950 K. For this test, the total temperature was held constant at 320 K. The test section and plenum chamber have multiple quartz windows to enable Schlieren and PSP measurement techniques in the facility. An interchangeable panel in the wind tunnel test section roof contains a germanium window, enabling IR measurements.

2.1. Acquisition equipment

2.1.1. Lighting. Lighting for this PSP experiment was delivered via a modified cheap ELEPHAS 3800 mini LCD projector shown in figure 3(a). The white LED in the projector was replaced with a Luminus Devices CBM-120-UV-C31-K395 LED, shown in figure 3(b). The UV LED has a similar form factor and allows for the use of the same heat sink and fan assembly requiring only small modifications without disturbing the copper heat pipes. The UV LED was powered

using a current-limited external bench power supply operating at 3.8 V, drawing 13 A, which was left to reach thermal equilibrium for approximately 10 min before acquisition. The projector consists of the LED output constrained by a reflective housing to increase the light hitting the Fresnel lens before the LCD. A further Fresnel lens (which can be actuated to remove keystone) passes the light onto a flat mirror before the beam passes out through the focusing and objective lenses. As with any commercial projector, individual pixels can be seen as small variations in the output intensity when the projector is in sharp focus.

The required wavelength of light to excite the PSP used is 395 nm, which is delivered via the LED. As the LED was placed in a projector with numerous lenses, Fresnel lenses and an LCD matrix, all of unknown material, the final output spectrum was measured using a Thorlabs CCS100 spectrometer to ensure that the part of the spectrum required for PSP excitation was not completely cut off. Figure 4 shows that the spectrum is not the expected Gaussian distribution centred around 395 nm (as per the LED datasheet) and instead shows some positive skew, i.e. the spectrum seems curtailed negative of the mean. This demonstrates that part of the useful LED spectrum has been effectively filtered by the projector optics; however, despite the projector optics removing part of the useful spectrum, the input signal is still close enough in wavelength to the PSP absorption wavelength and strong enough to excite the PSP.
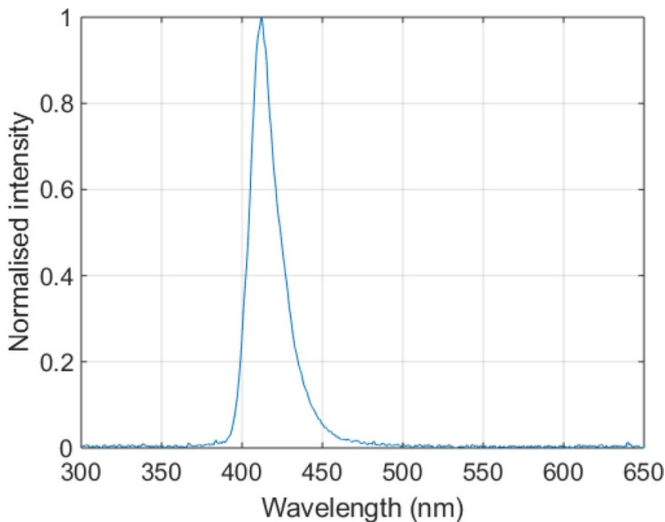
Figure 4. UV LED and projector spectrum.

When using the projector to create speckle patterns, the images sent to it were black and white. As the input light source is monochromatic, only modulation of a black and white signal was required to give UV patterns.

2.1.2. Imaging. The PSP and DIC data was recorded using a LaVision StrainMaster Portable system consisting of two 5 MP × 12 bit Imager E-lite CMOS cameras arranged on a heavy-duty Manfrotto tripod with a common mounting rail. The cameras were placed approximately 700 mm away from the model in the wind tunnel and fitted with 35 mm, f 1.6 c-mount lenses. The two cameras were separated by approximately 350 mm with a half angle of $\approx 15°$ between them. The lenses were fitted with M27 × 0.5 610 nm long-pass filters (with IR cut-off) manufactured by Galvoptics. The cameras were calibrated using the LaVision 106-10-SSDP calibration plate mounted inside the wind tunnel with the windows closed, giving an approximate image scale value of 15.8 pixels mm^{-1}. The cameras captured data at 2 Hz with an exposure time of 500 ms. Only a single image is recorded per condition.

As PSP measurements are sensitive to temperature, a FLIR A65SC camera mounted above the tunnel looking through the germanium window was used to monitor the model temperature during a run. The A65SC is a microbolometer-based detector which has a time constant of approximately 12 ms and captures data at 30 Hz using an in-house developed Lab-VIEW control algorithm. The emissivity of the surface was set to $\varepsilon = 0.95$ which is a typical value for matt painted surfaces and was validated by correlation with the ambient lab temperature on the model surface before the run commenced. The angle of the camera meant that the front (approximately) 10% of the model cannot be seen due to the nozzle blocking the camera view.

2.1.3. Pressure-sensitive paint. In order to thermally insulate the PSP from the model, improve the PSP adhesion, and to improve surface reflectivity, the model was cleaned with acetone and sprayed with a matt white acrylic-based paint before spraying with PSP. The PSP used in this experiment was the ISSI UniFIB PSP (0.7% per kPa and 0.5% per K published pressure and temperature sensitivity [35]) and was applied using a modeller's airbrush. The PSP was then cured in an oven for 6 h at 340 K in order to drive off any moisture and help set the coating. Following the curing process, the PSP-sprayed model was then placed in the HSST on the sting balance. During this time, the model was handled using cotton gloves to avoid contamination from human skin or other sources.

The PSP was calibrated by stepping through pressures using the HSST pressurisation system from vacuum up to 50 kPa in approximately 5 kPa steps, giving a calibration curve consistent with *a-priori* measurements seen previously [18] as shown in figure 5. The calibration coefficients were uniform across the entire image, meaning that there was no requirement for a pixel-wise calibration and that the model was very uniformly sprayed.

2.2. Image processing algorithm

After set-up and image capture, the images were processed using the StrainMaster package of DaVis 8.4. A rough geometric mask was applied to the images before processing in order to reduce the computational time required. Seeding points for the DIC algorithm were placed randomly on the image of the model surface. The images were then processed using a 31 pixel diameter subset mask with a step size of 13 pixels. Processing time was approximately 20 s on a standard Intel i5 laptop.

Once the surface data was calculated, it was exported as an XYZ point cloud into MATLAB. The PSP images were transformed using the Image Reconstruction algorithm in DaVis which projects the image intensity onto the same coordinate system as the surface mesh. The images were then exported as another XYZ point cloud with the Z data containing image counts.

As the model was manufactured using a high-precision CNC machine, the CAD geometry is taken as the ground truth for shape measurements. In order to facilitate comparison with measured data, a parametric grid of the model was generated in MATLAB as shown in figure 6. This mesh was evaluated at 12 M points and then projected using triangulation-based linear interpolation onto a regular mesh with the same number of points as the DIC data, giving an accurate mesh with a model nose-centred axis system.

In order to align the axis system of the DIC data to the ground truth of the flared cone model, a six degree of freedom rigid transformation was calculated using a singular value decomposition (SVD)-based iterative closest point (ICP) algorithm [36]. To speed up the process the SVD process, the data was masked to only include the model geometry and sub-sampled by a factor of three in the *x* and *y* directions leaving approximately 150 000 points for the ICP algorithm to align. The alignment process took approximately 4 min. Alternative algorithms, such as coherent point drift (CPD) [37], were also investigated; however the final aligned results were almost
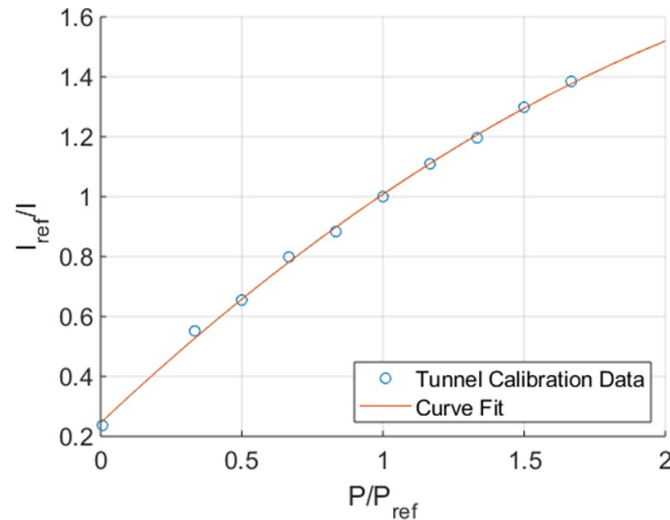
Figure 5. PSP calibration curve from tunnel data at $P_{ref} = 30$ kPa.
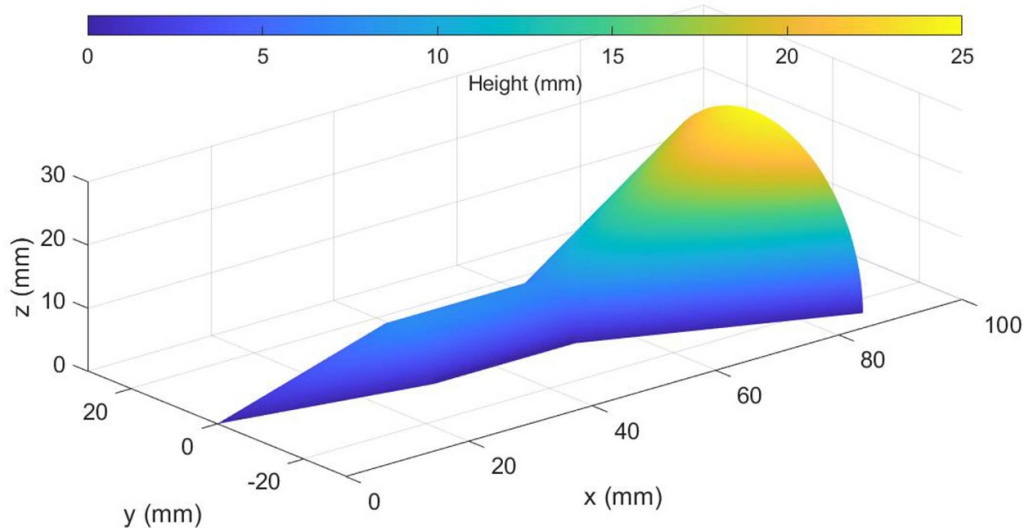

Figure 6. Ground truth of model mesh.

identical indicating that either algorithm would be suitable. This statement may not be true if there is large movement between the measured and CAD data, in this scenario a CPD algorithm may be more suitable.

The wind-on and -off PSP data was passed through a 3 pixel radius Gaussian filter and the calibration coefficients were applied. The surface required no extra post-processing and was immediately utilised in the format shown in figure 7(b).

Initial trials to measure the PSP and surface shape simultaneously used a random speckle pattern whilst having the projector in sharp focus, as can be seen in figure 7(a). Whilst this did produce a surface map with excellent clarity, even close to the edges of the model (figure 7(b)), the pattern does include areas of very low intensity, meaning that no PSP signal can be measured in this area (or that any measured signal will have a low signal-to-noise ratio), as shown in figure 9.

The random pattern applied was generated using a matrix of uniformly distributed random numbers with a threshold value,

creating a binary image. The threshold value could be adjusted easily and quickly to provide more or fewer *speckles*. There are approximately nine pixels (in a 3×3 array) per subset mask which provides sufficient texture at the resolution captured.

With PSP signal-to-noise ratio in mind, the projector was defocused by approximately 200 mm to provide an intensity level which was not zero at any location, but rather varied between white and mid-grey, as shown in figures 8(a) and 9. An alternative approach to solving this problem would be modulation of the intensity using the projector; however, this method still resulted in the pixel structure being strongly visible on the surface, still leading to dark areas when the projector is in sharp focus.

The surface mesh reconstructed from this defocused-projector image was very similar to the focused-projector mesh shown above. The difference in surface height between the two approaches is shown in figure 8(b). The central section of the surfaces i.e. closer to the DIC camera-normal plane, shows excellent agreement between the two meshes
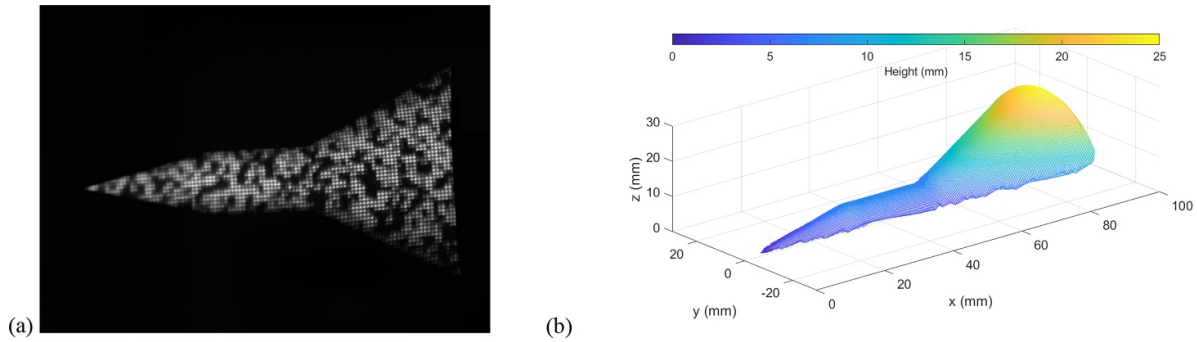
Figure 7. (a) Flared cone model with sharp focus projector; (b) surface mesh reconstruction presented with a subsampling factor of 5 in *x* and *y*.
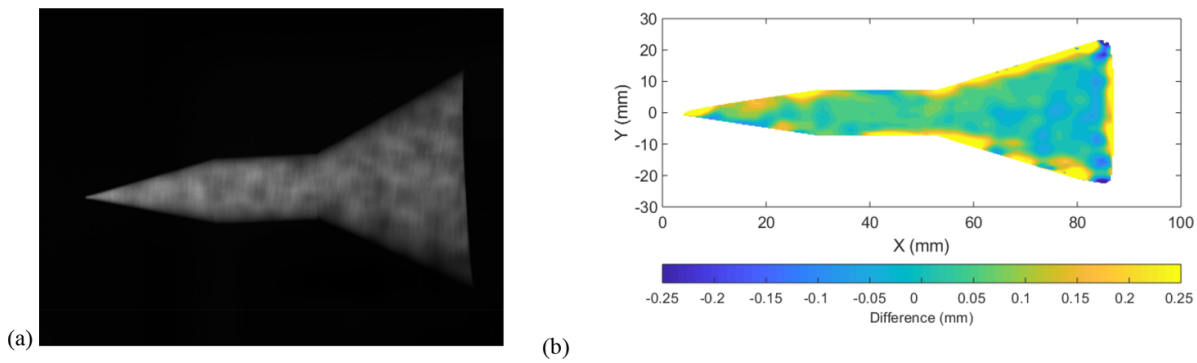

Figure 8. (a) Flared cone model with defocused projector; (b) difference between focused and defocused projector.
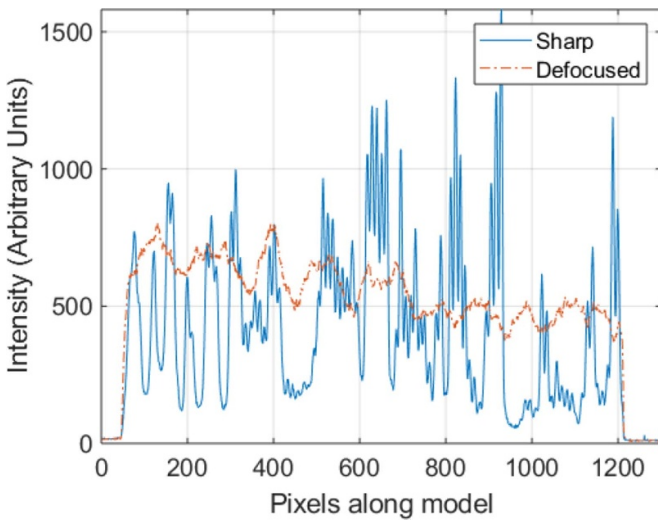

Figure 9. Intensity extracted along centreline of model from figures 7(a) and 8(a).

(differences smaller than 0.1 mm). Around the model edges there are more significant differences; however, given the strong curvature in these regions, this is not surprising. Approximately 120 degrees of the revolved model shape can be resolved accurately with the cameras in this orientation.

The centreline image intensity profile was extracted along the model from figures 7(a) and 8(a) and is plotted in figure 9. The texture present in the defocused line plot is sufficient

to reproduce a surface mesh from DIC. The large spikes in intensity and high levels of non-uniformity mean that the PSP signal from the sharp-focus line is significantly worse than that of the defocused line. Given that the defocused-projector images gave sufficient texture for DIC measurements and significantly better PSP response, they were used for all subsequent acquisition and processing.

2.3. Uncertainty analysis

Estimating the uncertainty contribution of all of the values in equation (1), the sensitivity of the results to their respective standard uncertainties can be calculated. This uncertainty analysis concludes that the standard uncertainty of the PSP is approximately 1.54 kPa in absolute terms or 1.02 in P/P_∞, where P is surface static pressure and P_∞ is freestream static pressure, as shown in figure 15.

The reference pressure, P_{ref} (nominally 26 kPa as recorded by the HSST control system), changes slowly over the course of the image acquisition due to the tunnel vacuum pumps re-evacuating the section for subsequent runs of the tunnel. This is estimated to have a rectangular distribution over a range of 1 kPa giving a standard uncertainty of 0.29 kPa.

In order to understand the contribution of temperature changes to the uncertainty in pressure, the sensitivity of the calibration coefficients to temperature was calculated using the *a-priori* calibration data for the same PSP formulation in the study by Quinn *et al* [18]. The temperature sensitivity coefficient was evaluated by calculating the total derivative of
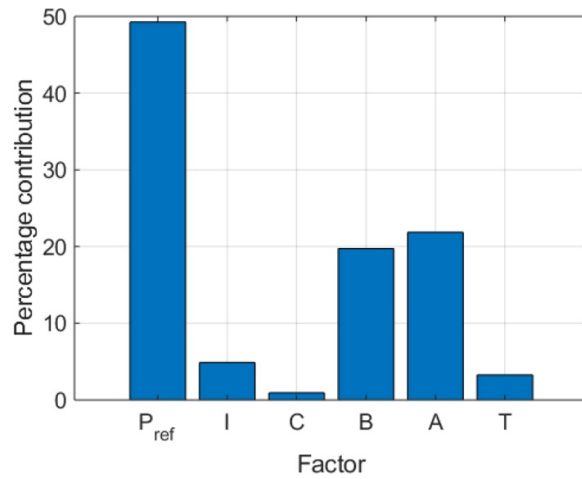
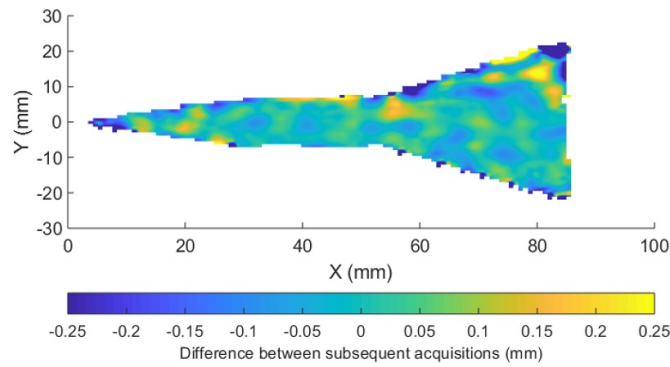**Figure 10.** Contribution of error sources in pressure results.

Figure 11. Difference between two wind-off mesh acquisitions visualised.
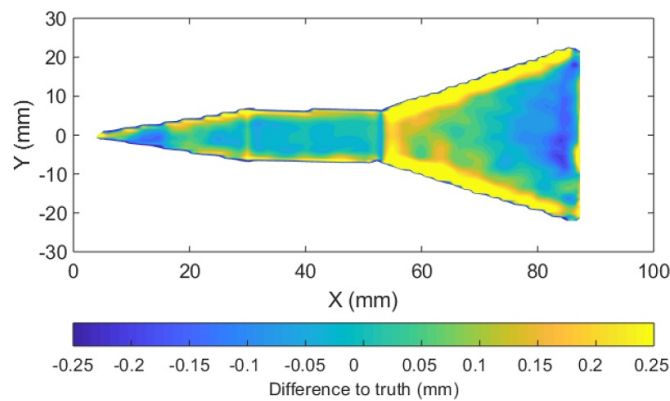

Figure 12. Difference between wind-on recorded mesh and ground truth after ICP transformation.

equation (1) with respect to temperature and evaluating the partial derivatives of each individual calibration coefficient with respect to temperature.

The reference pressure-induced uncertainties contribute approximately 50% of the total uncertainty in the result with the remainder coming from standard errors of curve fitting (evaluated from the variance matrix of least squares polynomial curve fitting) and camera noise (evaluated on the *in-situ* calibration images) as shown in figure 10.

Uncertainty in DIC data is slightly trickier to estimate (given the proprietary nature of the software) and as such approaches have been based on standard DIC practices. Standard DIC practice to evaluate noise on a measurement is to measure the same sample twice before any load has been applied and compare the differences. Ideally the differences should be zero; however, this is never the case. For this study, two wind-off measurements of surface shape were taken and the difference between them was subtracted. The standard
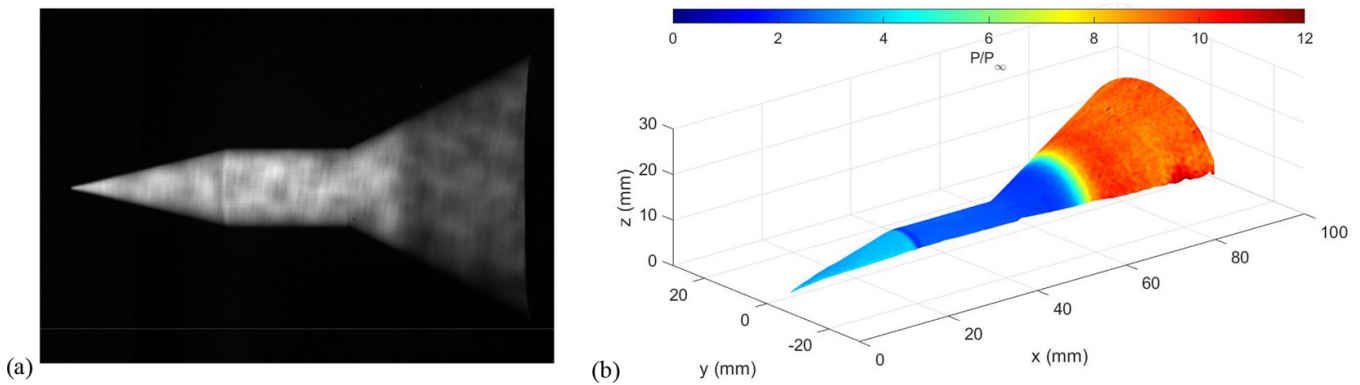
Figure 13. (a) Wind-on flared cone model with defocussed projector image; (b) PSP data and surface mesh reconstruction.

deviation of the difference between two acquisitions in the central 120 degrees of the model is 0.065 mm. The entire measured surface difference is shown in figure 11 again highlighting that uncertainties appear to be larger at the extremities of the mesh. It is worth noting that the regions of large discrepancy in figure 11 correspond to the darkest region of the surface of the model, indicating illumination strength also has a strong impact.

3. Results

In order to evaluate the accuracy of the surface mesh measurement, the algebraic model was compared to the measured surface using the wind-on images. There was negligible difference between the wind on and wind off images with the exception of a small rotation as measured by the ICP algorithm of 0.03 degrees in pitch and 0.28 degrees in yaw (this was measured by registering the wind-on and wind-off meshes). This difference produces a sub-pixel shift in the model location due to balance deflection. The difference between the presumed surface and the measured surface is shown in figure 12. If the results are restricted to the central section facing the camera the results are remarkably accurate showing agreement largely within 0.1 mm. The standard deviation of the difference shown in figure 12 between the truth and the measured mesh is 0.581 mm; however, if the measured data is masked to investigate only the centre section (approximately 120 degrees) the standard deviation is 0.094 mm. Given that the differences shown in figures 8(b), 11, and 12 are of the same order, and also given the HSST wind tunnel operates at low freestream density (approximately 0.1 kg m^{-3}), this indicates there are only minor aero-optical distortion effects in the surface mesh (or PSP) results. Previous studies in the facility using background oriented Schlieren on this model corroborate this [33]. The differences around the highly curved region of the flare section in figure 12 imply that aero-optical distortions in these areas are more significant than the more central 120 degree section. It is unsurprising that in these regions aero-optical distortions may become more significant as the camera views are effectively through highly curved shock waves in these regions.

The results shown in figure 13 are derived from using the wind-on image (figure 13(a)) to calculate the surface shape. This shape is used for the final data presentation shown in figure 13(b). The recompression shock shown in figure 1(b) is clearly visible in the raw wind-on PSP image in figure 13(a) despite the texture from the structured UV light field. The PSP data mapped on to the surface was captured by dividing figure 8(a) by figure 13(a). The results are presented as P/P_∞, i.e. surface pressure divided by freestream static pressure, as per previous studies [29, 38].

Figure 14(a) shows the temperature of the flared section of the model (post shock) during a run where the tunnel total temperature is set to 320 K as mentioned previously. The temperature change through the run is very modest with the measured temperature difference between wind-on and -off image acquisitions being approximately 0.1 K. The temperature profile across the model is shown in figure 14(b) where the reattachment and recompression region mentioned in figure 1(b) shows a higher temperature than the rest of the surface. Despite this increase, the maximum surface temperature deviation between wind-on and -off images is approximately 1 K as shown in figure 14(c).

In order to produce a more quantitative analysis, the surface pressure was extracted along the model centreline in figure 13(b) and is presented in figure 15. The values shown on this plot agree qualitatively with the results captured previously [29] and agree with simulation data [38] ndicating the reliability of the measurement. In the study by Shi *et al* [29] it was noted that CFD predicted the location of the reattachment point to be upstream of the measured location, as shown here (this was also demonstrated by Erdem [38]). This upstream impingement of the shear layer results from an over prediction of the expansion as seen between $0.35 < x/L < 0.65$ in figure 15.

4. Conclusion

This study has demonstrated a method of simultaneously measuring the surface shape and surface pressure distribution over an aerodynamic model without the need to interfere and damage a PSP coating. The use of a structured UV light field from a modified projector allowed for the
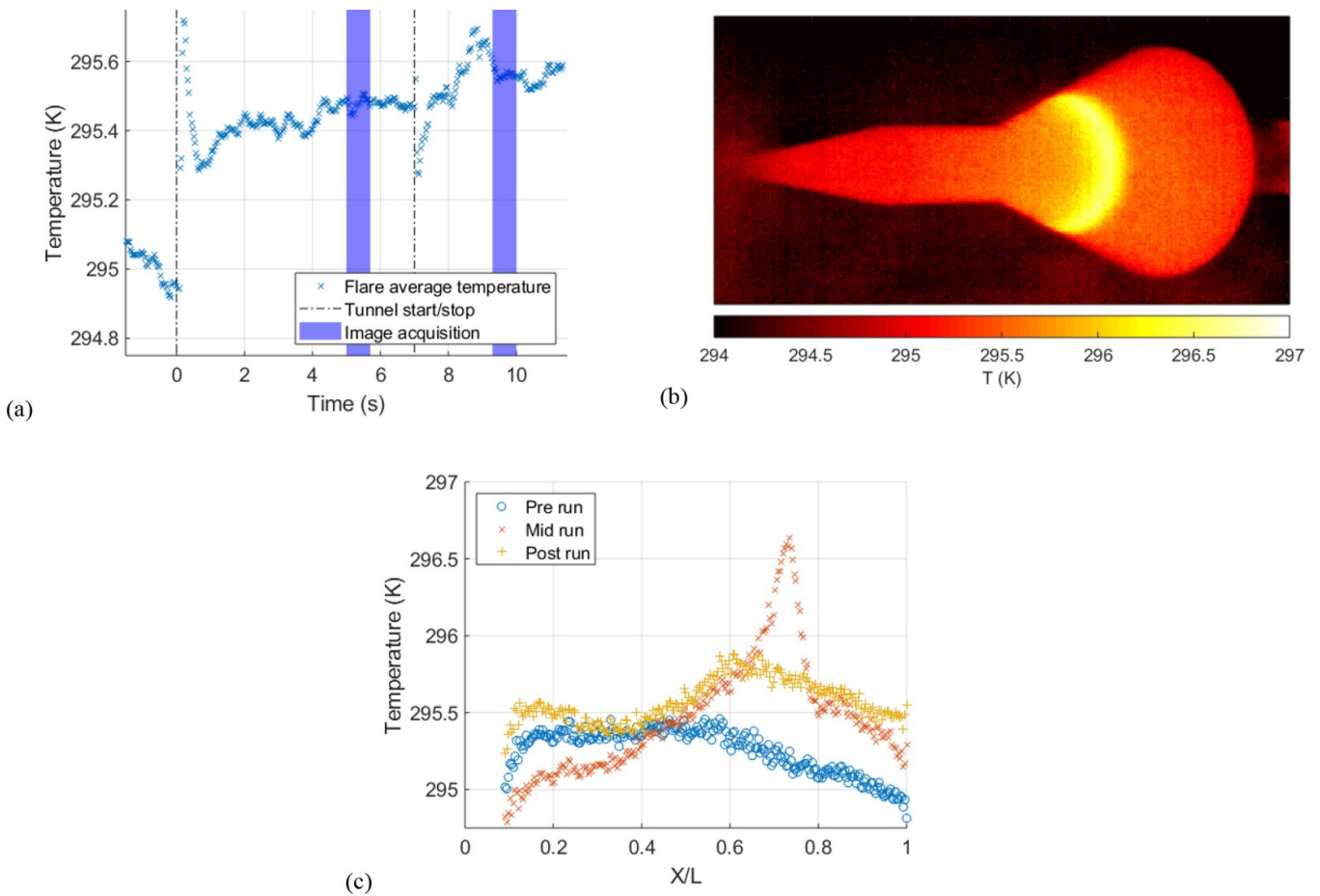
(a)

(b)

(c)

Figure 14. (a) Average temperature on the flared section (post shock) during a tunnel run; (b) temperature over the model surface at approximately 5 s during the run; (c) temperature profile from front to back along the model before, during and after the run.
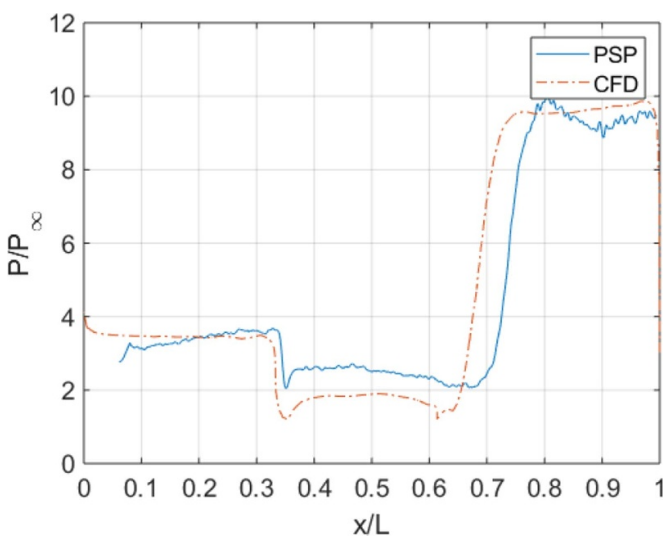

Figure 15. Centreline pressure distribution.

measurement of texture using a signal modulated with light rather than reflectivity or absorptivity. Measurements of surface shape were made that had sub-millimetre accuracy from a single snapshot, meaning that this could be improved if multiple images were captured, processed, and averaged. As the

PSP coating was uniformly applied, as is usually (hopefully) the case, the use of a structured light field does not introduce significant measurement errors as there was no vibration between excitation light and cameras. If vibration is present, sequential acquisition may be required in order to have measures of both pressure and shape without contamination of the PSP data. Large deformations in the model will require alternative approaches such as binary imaging; however, the method presented here is sufficient for small deflections or deformations. Significant out-of-calibration-plane motion would result in the textured light field producing artefacts in the PSP results unless illumination was generated by a collimated light source.

It was expected that the use of a structured light field for this application could be optimised for individual parts or components of a model by introducing regions of finer texture in regions of sharp changes in geometry. However, the DIC algorithm used (optical-flow-based least-squares matching) proved robust enough that surfaces could be reconstructed using little contrast in the incident light source. This has the added benefit of allowing the user to ensure that adequate lighting reaches every part of the PSP coating, yielding a much better signal-to-noise ratio from the PSP.

In order to capture an adequate signal for PSP, the exposure times of the cameras was rather long in this study. This was

due to the relatively low power of excitation light making it through the projector optical chain to the PSP. Alternative PSPs such as Ruthenium-based mixtures could be used as they respond to blue light rather than UV which will pass through the optical chain more readily. Future studies include using alternative luminophores and binary PSP formulations to increase the signal to noise ratio, lower the required exposure time, and reduce PSP temperature sensitivity.

This study demonstrates the possibility of performing fluid-structure interaction measurements using PSP and DIC simultaneously using one imaging system without compromising the PSP coating. With applicability to large-scale wind tunnel experimentation, having direct measurements of both surface pressure and shape simultaneously could have a significant cost saving for facilities which currently perform both measurements independently in different, expensive, wind tunnel campaigns.

Author contributions

Mark Quinn conceived the project. Mark Quinn and Tom Fisher jointly conducted the experimental campaign. Mark Quinn analysed the data and wrote the article, which was reviewed by both authors. Both authors were involved in development of the concepts investigated.

Acknowledgments

Conflicts of interest

The authors declare no conflict of interest.

ORCID iD

Mark K Quinn https://orcid.org/0000-0001-5788-4837

References

[1] Dowgwillo R, Morris M, Donovan J and Benne M, 1994 The application of the pressure sensitive paint technique to high speed wind tunnel testing of a fighter aircraft configuration with complex store loadings *12th Applied Aerodynamics Conference 20 June 1994 - 23 June 1994 Colorado Springs, CO* (https://doi.org/10.2514/6.1994-1932)

[2] Sellers M 2000 Application of pressure sensitive paint for determining aerodynamic loads on a scale model of the F-16C *21st Aerodynamic Measurement Technology and Ground Testing Conference 19 June 2000 - 22 June 2000 Denver, CO* (https://doi.org/10.2514/6.2000-2528)

[3] Klein C, Engler R H, Henne U and Sachs W E 2005 Application of pressure-sensitive paint for determination of the pressure field and calculation of the forces and moments of models in a wind tunnel *Exp. Fluids* **39** 475–83

[4] Nakakita K, Kurita M, Mitsuo K and Watanabe S 2006 Practical pressure-sensitive paint measurement system for industrial wind tunnels at JAXA *Meas. Sci. Technol.* **17** 359–66

[5] Vardaki E, Stokes N, Patel S and Gustafsson P 2012 Pressure sensitive paint measurements on the Gripen Model at the ARA transonic wind tunnel *50th AIAA Aerospace Sciences Meeting including the New Horizons Forum and Aerospace Exposition 09 January 2012 - 12 January 2012 Nashville, Tennessee* (https://doi.org/10.2514/6.2012-1188)

[6] Roozeboom N H *et al* 2019 Development of unsteady pressure-sensitive paint application on NASA Space Launch System *AIAA Aviation 2019 Forum 17-21 June 2019 Dallas, Texas* (https://doi.org/10.2514/6.2019-3502)

[7] Liu T and Sullivan J P 2005 *Pressure and Temperature Sensitive Paints* (Berlin: Springer)

[8] Kameda M, Tabei T, Nakakita K, Sakaue H and Asai K 2005 Image measurements of unsteady pressure fluctuation by a pressure-sensitive coating on porous anodized aluminium *Meas. Sci. Technol.* **16** 2517–24

[9] Gregory J W, Asai K, Kameda M, Liu T and Sullivan J P A review of pressure-sensitive paint for high-speed and unsteady aerodynamics 2008 *J. Aerosp. Eng.* **222** 249–90

[10] Quinn M K, Yang L and Kontis K 2011 Pressure-sensitive paint: effect of substrate *Sensors* **11** 11649–11663

[11] Peng D and Liu Y 2019 Fast pressure-sensitive paint for understanding complex flows: from regular to harsh environments *Exp. Fluids* **61** 8

[12] Flaherty W, Reedy T M, Elliott G S, Austin J M, Schmit R F and Crafton J 2014 Investigation of cavity flow using fast-response pressure-sensitive paint *Aiaa J.* **52** 2462–70

[13] Roberts D A, Stokes N P, Quinn M K, Coppin J and Birch T J 2016 Evaluation of dynamic pressure-sensitive paint for improved analysis of cavity flows and CFD validation *54th AIAA Aerospace Sciences Meeting 4-8 January 2016 San Diego, California, USA* (https://doi.org/10.2514/6.2016-0311)

[14] Sellers M, Nelson M and Crafton J 2016 Dynamic pressure-sensitive paint demonstration in AEDC propulsion wind tunnel 16T *54th AIAA Aerosp. Sci. Meet.* pp 1–36

[15] Crafton J, Stanfield S, Rogoshchenkov N and Schmit R 2017 Investigation of passive flow control of cavity acoustics using dynamic pressure-sensitive paint *55th AIAA Aerospace Sciences Meeting 9–3 January 2017 Grapevine, Texas* (https://doi.org/10.2514/6.2017-1178)

[16] Allen N J and Quinn M K 2015 Development of a transonic gust rig for simulation of vertical gusts on half-models *31st AIAA Aerodynamic Measurement Technology and Ground Testing Conference 22-26 June 2015 Dallas, TX* (https://doi.org/10.2514/6.2015-2403)

[17] Quinn M K and Kontis K 2013 Pressure-sensitive paint measurements of transient shock phenomena *Sensors (Switzerland)* **13** 4404–27

[18] Quinn M K, Spinosa E and Roberts D A Miniaturisation of pressure-sensitive paint measurement systems using low-cost, miniaturised machine vision cameras 2017 *Sensors* **17** 1–21

[19] Quinn M K 2018 Binary pressure-sensitive paint measurements using miniaturised, colour, machine vision cameras *Meas. Sci. Technol.* **29** 055107

[20] Vardaki E, Stokes N, Fonov S and Crafton J 2010 Pressure sensitive paint measurements at the ARA transonic wind tunnel *27th AIAA Aerodynamic Measurement Technology*

and Ground Testing Conference 28 June 2010 - 01 July 2010 Chicago, Illinois (https://doi.org/10.2514/6.2010-4796)

[21] Davidson T S, Stokes N P, Roberts D A and Quinn M K 2019 Time-resolved surface pressure and model deformation measurements in an industrial transonic wind tunnel

[22] Sakaue H, Miyamoto K and Miyazaki T 2013 A motion-capturing pressure-sensitive paint method *J. Phys. D: Appl. Phys.* **113** 084901

[23] Hayashi T, Houpt A W, Leonov S B and Sakaue H 2019 Motion-capturing pressure-sensitive paint method under transient illumination by plasma source *J. Phys. D: Appl. Phys.* **52** 324005

[24] Disotell K J and Gregory J W 2011 Measurement of transient acoustic fields using a single-shot pressure-sensitive paint system *Rev. Sci. Instrum.* **82** 075112

[25] Disotell K J, Peng D, Juliano T J, Gregory J W, Crafton J W and Komerath N M 2014 Single-shot temperature- and pressure-sensitive paint measurements on an unsteady helicopter blade *Exp. Fluids* **55** 1671

[26] Weiss A *et al* 2017 Single-shot pressure-sensitive paint lifetime measurements on fast rotating blades using an optimized double-shutter technique *Exp. Fluids* **58** 120

[27] Dong Z, Liang L, Zhang W, Jiao L, Peng D and Liu Y 2020 Simultaneous pressure and deformation field measurement on helicopter rotor blades using a grid-pattern pressure-sensitive paint system *Measurement* **152** 107359

[28] Ogg D R, Rice B E, Peltier S J, Staines J T, Claucherty S L and Combs C S 2018 Simultaneous stereo digital image correlation and pressure-sensitive paint measurements of a compliant panel in a mach 2 wind tunnel (https://doi.org/10.2514/6.2018-3869)

[29] Shi S, Xu S, Zhao Z, Niu X and Quinn M K 2018 3D surface pressure measurement with single light-field camera and pressure-sensitive paint *Exp. Fluids* **59** 79

[30] Lynch K P, Jones E M and Wagner J L 2018 Simultaneous PSP and DIC measurements for fluid-structure interactions in a shock tube (https://doi.org/10.2514/6.2018-3870)

[31] Ravichandran R, Gramola M and Bruce P J 2020 Simultaneous pressure and displacement measurements on a 3D flexible surface in a supersonic flow (https://doi.org/10.2514/6.2020-0315)

[32] Gramola M, Bruce P J and Santer M J 2020 Response of a 3D flexible panel to shock impingement with control of cavity pressure (https://doi.org/10.2514/6.2020-0314)

[33] Fisher T, Quinn M K and Smith K 2019 An experimental sensitivity comparison of the Schlieren and background-oriented Schlieren techniques applied to hypersonic flow *Meas. Sci. Technol.* **30** 065202

[34] Erdem E, Yang L and Kontis K 2011 Drag Reduction Studies by Steady Energy Deposition at Mach 5 (https://doi.org/10.2514/6.2011-1027)

[35] Innovative Scientific Solutions Incorporated 'UniFIB Pressure Sensitive Paint Data Sheet' (www.psp-tsp.com/PDFs/Paint-Data-sheets/UniFIB-PSP-UF-XXX-Data-Sheet.pdf)

[36] Wilm J 2020 'Iterative Closest Point' MATLAB Central File Exchange (www.mathworks.com/matlabcentral/fileexchange/27804-iterative-closest-point)

[37] Myronenko A and Song X 2010 Point set registration: Coherent point drifts *IEEE Trans. Pattern Anal. Mach. Intell.* **32** 2262–75

[38] Erdem E 2011 Active Flow Control Studies at Mach 5: Measurement and Computation University of Manchester